Effect of Solvent Quality on the Rheological and Rheooptical Properties of Flexible Polymer Solutions

N. C. Andrews, A. K. Doufas, and A. J. McHugh*

Department of Chemical Engineering, University of Illinois at Urbana−Champaign, Urbana, Illinois 61801

Received September 15, 1997; Revised Manuscript Received February 18, 1998

ABSTRACT: The dynamics of dilute solutions of flexible polymer molecules with intramolecular excluded volume interactions are modeled using nonequilibrium Brownian dynamics (NEBD) and configuration-biased Monte Carlo (CBMC) simulations. The mathematical model consists of beads interacting through stretching and excluded volume forces under both shear and extensional flow. Various conformational and rheological quantities, such as birefringence, mean squared end-to-end distance, and viscosities, are calculated for steady-state and transient flows, with the primary independent variable being the *solvent quality e**. The model predicts coil−stretch transitions in extensional flow. The molecular weight scaling of the critical extension rate is found to vary as $M^{-1.6}$ under poor solvent conditions and M^{-2} in a good solvent, in qualitative agreement with experiments reported in the literature. Model calculations also qualitatively capture a number of other observed features, most notably higher elongational viscosities under good solvent conditions and faster relaxation behavior under poor solvent conditions.

Introduction

Solvent quality can have a dramatic effect on the conformational state of a macromolecule. The effect of solvent quality on the static-equilibrium conformational behavior is well-established;[1] however, the transient behavior, especially rheological, is still rather poorly understood. Good solvent conditions imply dominance of the repulsive intramolecular interactions (or, equivalently, excluded volume interactions) between the beads of the chain and, therefore, a swollen state of the polymer. Poor solvent conditions dictate the controlling influence of the attractive intramolecular interactions and, therefore, imply a collapsed state of the polymer. For each polymer−solvent system, there is a critical temperature (Θ temperature) at which the attractive and repulsive interactions cancel out. It is obvious that above the Θ temperature, chains will be in a swollen state, while below the Θ temperature, they will be in a collapsed state.

Solvent quality may be modeled through the effect of a "solvent-mediated" force between the beads. A standard potential often used is the Lennard-Jones potential;[2] however, this is computationally taxing for Brownian dynamics simulations owing to the small time steps required.[3] An alternative is the Morse potential,[3,4] which has properties very similar to a Lennard-Jones potential, yet allows less dramatic changes in the time-step size. Numerous equilibrium computational studies[5−13] have been carried out, in which the aim has been numerical determination of the Θ temperature and investigation of the configurational state of the polymer chain below and above this temperature. Various static properties were determined such as the mean squared end-to-end distance, mean squared radius of gyration, and intrinsic viscosity. Most of these calculations were based on variations of the Monte Carlo method (lattice,[5,7,11,12] off-lattice,[6,8−10] and configuration-biased Monte Carlo sampling procedures[13]). The only simulation that we are aware of that deals with the *dynamics* under no-flow conditions is the dissipative particle dynamics simulation of Kong et al.,[14] which demonstrated that polymers in a good solvent take a longer time to relax than those in poor solvent conditions.

While some experimental work has been done on the effect of solvent quality (or temperature change) on the mechanical and optical transient response of flexible polymer solutions in elongational flows,[15−18] very little, if any, work has been done on the modeling and theoretical investigation of these dynamical effects. The motivation of the current study has therefore been to understand the effect of solvent quality on the *transient* rheological and rheooptical dynamics, especially viscosity and birefringence, in both shear and extensional flows. In our calculations, configuration-biased Monte Carlo (CBMC) simulations are utilized to obtain the Θ temperature and nonequilibrium Brownian dynamics (NEBD) are used to model the dynamics.

Theory and Methods

(a) Model. The polymer chain is modeled as N identical beads of mass m, connected by flexible "Fraenkel" springs of equilibrium length Q_0 with the *stretching* potential energy U^S given by

$$U^S = \sum_{i=1}^{i=N-1} \frac{1}{2}\alpha' k_B T(|\boldsymbol{Q}_i| - Q_0)^2 \qquad (1)$$

where α' is the stretching constant, k_B is Boltzmann's constant, and T is the temperature. The position vector of the ith bead with respect to a laboratory frame is denoted by $\boldsymbol{r}_i$, and the vector representing each link (or segment) is given by $\boldsymbol{Q}_i = \boldsymbol{r}_{i+1} - \boldsymbol{r}_i$. Each bead has a radius given by a which is some fraction of Q_0, depending on the extent of hydrodynamic interactions (i.e., for the *touching bead* model, used by many researchers,[19] where the hydrodynamic interaction is the strongest; $Q_0 = 2a$). Intramolecular excluded volume interactions are represented by the Morse potential, given by[4]

* To whom correspondence should be addressed.

S0024-9297(97)01359-4 CCC: $15.00
Published on Web 04/08/1998

$$U^{EV} = e \sum_{i=1}^{i=N-1} \sum_{j=i+1}^{j=N} \exp[-2a(r_{ij} - r_{min})] - 2\exp[-a(r_{ij} - r_{min})] \quad (2)$$

where $r_{ij} = |\mathbf{r}_i - \mathbf{r}_j|$ and a, r_{min}, and e are parameters.

(b) Numerical Methods. The Fokker−Planck diffusion equation for the probability distribution of the beads in the chain is used to derive the stochastic differential equation (SDE) governing their positions, which reads[21]

$$d\mathbf{r}_i = \left[\mathbf{K}\cdot\mathbf{r}_i + \frac{1}{\zeta^t}(\mathbf{f}_i^S + \mathbf{f}_i^{EV}) + \sum_j \boldsymbol{\Omega}_{ij}\cdot(\mathbf{f}_j^S + \mathbf{f}_j^{EV}) + \frac{k_B T}{\zeta^t}\sum_j \frac{\partial}{\partial \mathbf{r}_j}\cdot\boldsymbol{\gamma}_{ij}\right] dt + \sqrt{\frac{2k_B T}{\zeta^t}}\sum_j \mathbf{B}_{ij}\cdot d\mathbf{W}_j \quad (3)$$

where $\boldsymbol{\gamma}_{ij} = \boldsymbol{\Omega}_{ij} + \delta_{ij}\mathbf{I}$, $\boldsymbol{\Omega}_{ij}$ is the Rotne−Prager−Yamakawa hydrodynamic interaction tensor,[22] $\mathbf{K}$ denotes the transpose of the velocity gradient tensor, ζ^t is the translational friction coefficient ($6\pi\eta_S a$, η_S being the solvent viscosity), and $\mathbf{f}_i^S$ and $\mathbf{f}_i^{EV}$ are, respectively, the stretching and excluded volume forces, obtained by taking the derivative with respect to $\mathbf{r}_i$ of eq 1 or eq 2, respectively. $d\boldsymbol{W}_j$ represents a vector of independent Wiener processes, and $\boldsymbol{B}_{ij}$ is a matrix representing the covariance of the particle displacements.[21] To implement the NEBD algorithm, one starts with eq 3 and forward integrates using a second-order predictor−corrector scheme.[20] In the results to be presented, hydrodynamic interactions have been neglected, since we have found that their inclusion changes the results only quantitatively, while the qualitative trends are maintained.

For each set of parameter values, a time-step extrapolation procedure was performed to guarantee the solution stability. Due to the rather steep nature of the potential, and hence large forces, a dimensionless time step of 10^{-5} was used in the simulations. For each time step, an ensemble of 1000 chains was used to generate running averages and variances. Unless otherwise stated, a bead number of 10 was used. To obtain steady-state averages, standard block averaging and error analysis were used.[2,20] In addition, the variance reduction procedure of Wagner and Öttinger[23] was used to reduce the noise in our simulations.

Initial chain configurations were generated using the CBMC procedure which utilizes the equilibrium stretching and excluded volume energy terms. CBMC was also used for the elongational flow calculations, since, in this case, one has the analytic solution of the probability diffusion equation given by[24]

$$\Psi = \frac{1}{J}\exp\left[-\frac{U^S}{k_B T} - \frac{U^{EV}}{k_B T} + \frac{\zeta^t}{2k_B T} K_{\alpha\beta}\left(\sum_{ij} C_{ij}\boldsymbol{Q}_i\boldsymbol{Q}_j\right)_{\beta\alpha}\right] \quad (4)$$

where J is a normalization constant and C_{ij} is the Kramers matrix. For initial chain generation, the equilibrium distribution function, given by eq 4 without the third term inside the exponent, was used. Further details on the algorithm can be found in our earlier work.[25] A typical simulation run consisted of between 10^5 and 10^6 cycles, and during each cycle, the chain was grown 10 times, with the number of trial segments being 8. Averages were performed in blocks, the typical block size being 1000 cycles (1 out of every 10 of which is used to compute the averages within a block).

Both shear and elongational flows were considered; in shear flow, the solvent velocity field is given by $v_x^S = \dot{\gamma}y$, $v_y^S = 0$, and $v_z^S = 0$, where $\dot{\gamma}$ is the shear rate, and in uniaxial extensional flow, the principal flow direction is in the x direction, with the 11, 22, and 33 components of the velocity gradient tensor being $\dot{\epsilon}$, $-\dot{\epsilon}/2$, and $-\dot{\epsilon}/2$ respectively, where $\dot{\epsilon}$ is the homogeneous extension rate.

(c) Dimensionless Parameters. It is convenient to nondimensionalize our equations; the resulting dimensionless parameters are (i) lengths, which are nondimensionalized by Q_0, for example, a dimensionless length $\boldsymbol{Q}_i^* = \boldsymbol{Q}_i/Q_0$; (ii) the dimensionless stretching constant $\alpha = \alpha' Q_0^2$; (iii) the dimensionless time $t^* = tk_B T/\zeta^t Q_0^2$; (iv) the dimensionless elongational (or shear) rate ϵ (or γ) $= \dot{\epsilon}(\dot{\gamma})\ \zeta^t Q_0^2/k_B T$; (v) the dimensionless solvent quality parameter $e^* = e/k_B T$; (vi) the dimensionless parameters of the Morse potential, $a^* = a/Q_0$ and $r_{min}^* = r_{min}/Q_0$, and (vii) the bonded potential, which is nondimensionalized with respect to $k_B T$, i.e., $U^{*S} = U^S/k_B T$.

The stretching constant α has been given a value of 1000 in all of our simulations, as this represents a rather stiff spring, such that an unphysical stretching of the contour length is prevented.[26] Concerning the dimensionless parameters of the Morse potential, a^* has been assigned a value of 5 and r_{min}^* a value of 0.9, while the solvent quality parameter e^* has been varied in the range 0−3.

(d) Macroscopic Parameters. The parameters we monitor in our simulations are the following: (1) *the birefringence*, given by the difference in principle eigenvalues of the birefringence tensor, which reads

$$\Delta\mathbf{n}' = {}^2/_9\pi\nu\frac{(\tilde{n}^2+2)^2}{\tilde{n}}(\alpha_1 - \alpha_2)Q_0^2\sum_{i=1}^{N-1}\langle\boldsymbol{Q}_i^*\boldsymbol{Q}_i^*\rangle \quad (5)$$

where α_1 and α_2 denote the polarizabilities of the molecular segments, $\tilde{n}$ is the average solution refractive index, and ν is the number density of molecules; in our simulations, we use a reduced birefringence tensor, in which eq 5 is divided by the proportionality constant, C_b, given by

$$C_b = {}^2/_9\pi\nu\frac{(\tilde{n}^2+2)^2}{\tilde{n}}(\alpha_1 - \alpha_2)Q_0^2 \quad (6)$$

(2) *the dimensionless mean square end-to-end distance* $\langle R^2\rangle$, given by $(\mathbf{r}_N - \mathbf{r}_1)^2$ and its equilibrium value, denoted as $\langle R_0^2\rangle$; (3) the polymer contribution to the *stress tensor*, which is calculated using the Kramers expression[24]

$$\boldsymbol{\Pi}_p = \sum_{i=1}^{N-1}\langle\boldsymbol{Q}_i^*\mathbf{F}_i^{*(c)}\rangle \quad (7)$$

where $\mathbf{F}_i^{*(c)}$ is the connector tension defined as

$$\mathbf{F}_i^{*(c)} = -\frac{\partial(U^{*S} + U^{*EV})}{\partial\boldsymbol{Q}_i^*} \quad (8)$$

(4) the *shear viscosity* and *first normal stress coefficient*, given, respectively, by

$$\eta = \frac{\Pi_{p,xy}}{\gamma} \tag{9}$$

and

$$\psi_1 = \frac{\Pi_{p,xx} - \Pi_{p,yy}}{\gamma^2} \tag{10}$$

and (5) the *extensional viscosity*, η_E, given by

$$\eta_E = \frac{\Pi_{p,xx} - \Pi_{p,zz}}{\epsilon} \tag{11}$$

Results and Discussion

(a) Determination of the Θ Point. Figure 1 shows the CBMC simulation results for the equilibrium mean squared end-to-end separation (divided by $N - 1$) as a function of the solvent quality parameter e^* for various bead numbers N. The point of intersection of all curves is the Θ point,[10] about 0.32 as seen in Figure 1. These curves clearly display characteristics of a collapse transition, with the higher N values displaying a sharper transition. It should be noted that the intersection of the various N curves occurs for $N > 8$. In the calculations to be presented, chains of 10−18 beads were used since these intersect the corresponding curves of the higher N chains in Figure 1. Moreover, from our previous work on such chains,[20,25−27] the N values used here are well within the range used to obtain numerous features of the chains, both in statics and transient dynamics. Simulations were carried out below and above the value of e^* at the Θ point to simulate good ($e^* = 0.1$) and poor ($e^* = 3.0$) solvent conditions, respectively.

(b) Extensional flow calculations. Figures 2 and 3 show the steady-state birefringence and mean squared end-to-end distance behavior, respectively, as a function of elongation rate in a good and a poor solvent. Larger values of the birefringence in the good solvent reflect the more expanded state of the chain. However, in either solvent, due to the inherent flexibility, above some critical extension rate, an apparent coil−stretch transition occurs. In either solvent, the birefringence as well as the mean squared end-to-end separation remains relatively unaffected for a range of extension rates, indicating the dominance of the intramolecular forces over the hydrodynamic forces. However, at higher extension rates, a dramatic increase occurs. One also sees that, for high values of the extension rate, the birefringence asymptotically approaches the same limiting behavior in either solvent (Figure 2), reflecting the fact that the chain end-to-end separation under these conditions is essentially the same (Figure 3). The chain length (molecular weight) dependence of the extensional flow dynamics in a good solvent is illustrated in Figure 4.

The effect of solvent quality on the coil−stretch transition in dilute polystyrene solutions has been studied by Nguyen et al.[16] and Narh et al.[17] using the opposing jets apparatus. Our simulations indicate that on the average $\epsilon_c \sim M^{-1.6}$ in a poor solvent and $\epsilon_c \sim M^{-2}$ in a good solvent (see Figure 4), in qualitative agreement with the experiments of Nguyen et al.[16] Our scaling exponents were estimated based on linear regression fits of the critical extension rates vs molecular weight (logarithmic quantities). Although the correlation coefficients were found to be satisfactorily high, due to the relatively small statistical sample, only average values of the exponents have meaning; however, the model does capture the correct qualitative trends. Narh et al.[17] also found that the longest relaxation time of the molecule, given by the inverse of ϵ_c, increased with increasing solvent quality. This feature is shown in our simulations as well. From Figures 2 and 4, the dimensionless relaxation times for the 10-bead chain in the poor and good solvents are found to be about 0.77 and 3.7, respectively.

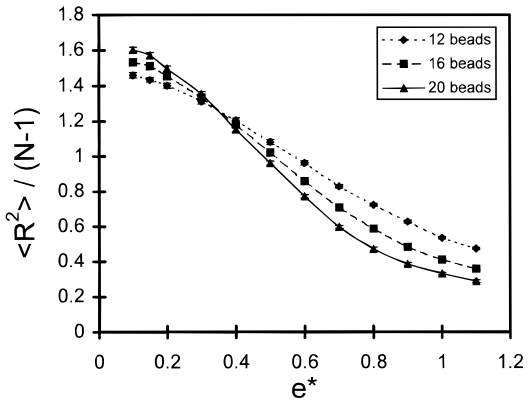

Figure 1. Normalized mean squared end-to-end distance, $\langle R^2 \rangle/(N - 1)$, vs solvent quality parameter e^* for the determination of the Θ point by CBCM simulations. N represents the chain number of beads. Error bars appearing in this and the following figures indicate the numerical errors of the simulations.

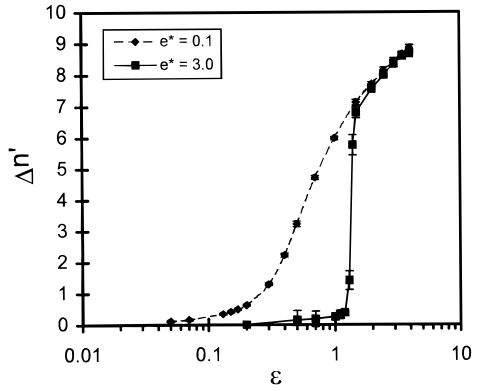

Figure 2. Steady-state birefringence vs extension rate for a good and a poor solvent. The number of beads, N, per chain in this and the remaining figures is 10, unless otherwise stated. Moreover, in this and following figures, $e^* = 0.1$ and $e^* = 3.0$ imply good and poor solvent conditions, respectively.

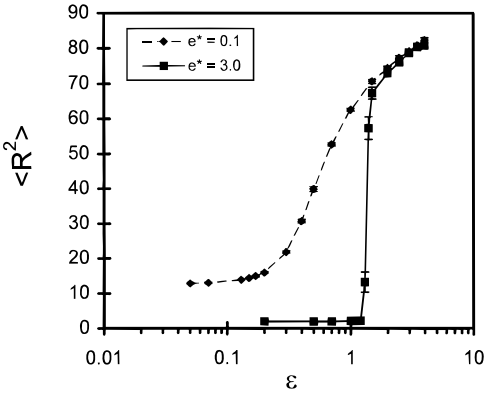

Figure 3. Steady-state mean squared end-to-end distance vs extension rate for a good and a poor solvent.

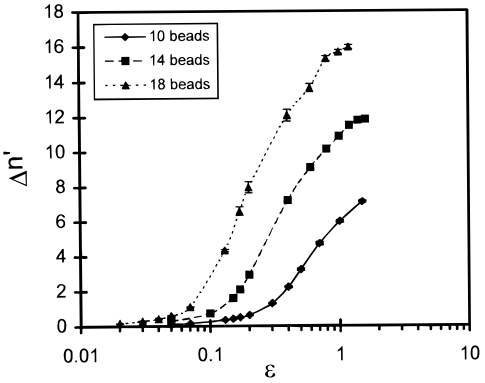

Figure 4. Steady-state birefringence vs extension rate for a good solvent for chains of various bead numbers.

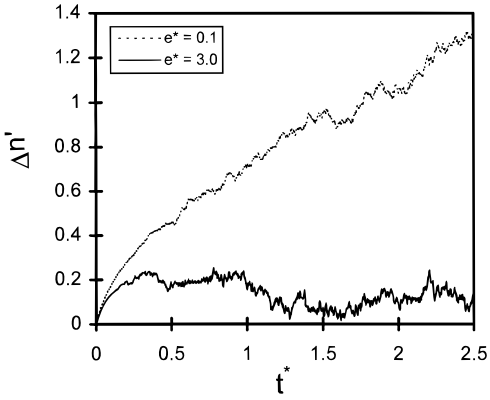

Figure 5. Transient birefringence in a good and a poor solvent for $\epsilon = 0.5$.

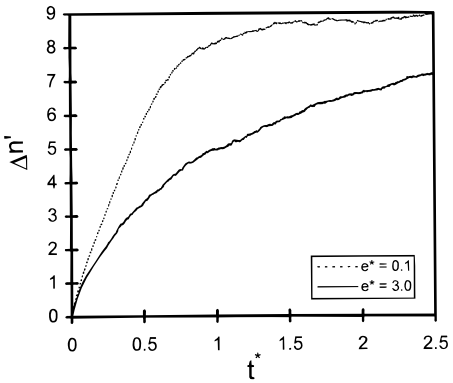

Figure 6. Transient birefringence in a good and a poor solvent for $\epsilon = 4$.

The transient birefringence for a relatively low extension rate (0.5) in both solvents is shown in Figure 5. A similar pattern is found for the end-to-end separation. Since the elongation rate is below the critical value for the poor solvent, the chain remains in a more-or-less collapsed state during flow. However, as expected, for extension rates greater than the critical value in both solvents, much more dramatic changes occur. For example, as shown in Figures 6 and 7, the birefringence and extensional viscosity rise more rapidly and display higher values in a good solvent. Both of these trends are in agreement with experimental findings.[15,18]

(c) Shear Flow Calculations. Figure 8 shows the transient birefringence for varying solvent quality and shear deformation. The effect of solvent quality on birefringence is seen to be stronger for the lower shear rate of 20. For example, an average change of the

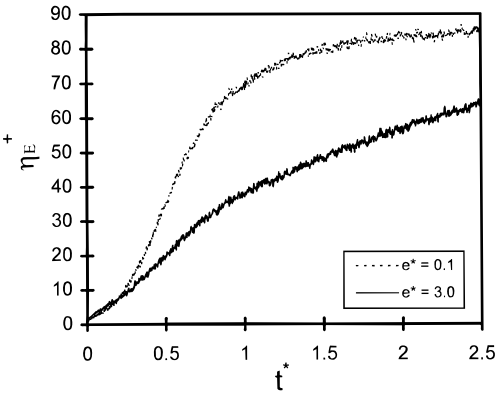

Figure 7. Transient elongational viscosity, n_E^+, associated with startup of flow, in a good and a poor solvent for $\epsilon = 4$.

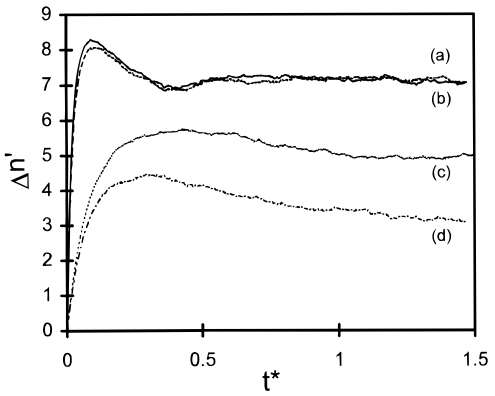

Figure 8. Effect of solvent quality on the transient birefringence for various shear rates: (a) $e^* = 0.1$, $\gamma = 100$; (b) $e^* = 3.0$, $\gamma = 100$; (c) $e^* = 0.1$, $\gamma = 20$; and (d) $e^* = 3.0$, $\gamma = 20$.

transient birefringence in the poor solvent relative to the good one is about 40% at the shear rate of 20 and only 1% at the shear rate of 100. This can be attributed to the fact that in the regime of very high shear rates, hydrodynamic forces overcome the intramolecular interactions and, therefore, the flow more-or-less governs the dynamics of the chains. This is in agreement with Figure 2, where the steady-state birefringence approaches almost the same value for high extension rates. Similar behavior was found to be valid for the mean squared end-to-end separation and the first normal stress coefficient, while the shear viscosity was seen to be practically insensitive to solvent quality for all the range of shear rates studied (figures not shown). Furthermore, as shown in Figure 8, the birefringence overshoots are much sharper for the high dimensionless shear rate of 100 and shift toward smaller times, consistent with our previous results for relatively flexible molecules with no intramolecular interactions.[20]

(d) Cessation of Flow Calculations. An example of the relaxation behavior of the normalized birefringence following extensional flow cessation is shown in Figure 9. Similar results occur for the mean squared end-to-end separation. As seen in Figure 9, the chain in the poor solvent relaxes faster, which is in agreement with the intrinsic relaxation time behavior found in the experiments of Kong et al.[14] and Narh et al.[17] The same qualitative trends were also found in our calculations for the molecular relaxation following cessation of shear flow.

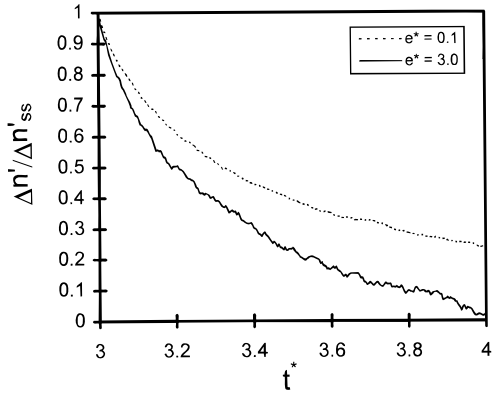

Figure 9. Effect of solvent quality on the birefringence relaxation following cessation of an extensional flow of $\epsilon = 2.3$. Flow is turned off at a dimensionless time of 3. The subscript "ss" refers to the value of the birefringence at the cessation of flow.

Conclusions

Our computations have enabled us to quantify the effect of solvent quality on the dynamics of dilute solutions of flexible chains. The effect of solvent quality on birefringence, mean squared end-to-end distance, and first normal stress coefficient is stronger in the low shear rate regime, while the shear viscosity is essentially unaffected by solvent quality for all the shear rates studied. In transient elongational flow, both the birefringence and viscosity are strongly affected by the quality of the solvent, with calculated trends in agreement with experimental observations reported in the literature. Model calculations also predict coil−stretch transitions in extensional flow with the critical extension rate scaling with molecular weight as $\sim M^{-1.6}$ in a poor solvent and $\sim M^{-2}$ in a good solvent. Cessation behavior following either shear or extension also reveals that chains in a poor solvent relax faster than in a good one.

Acknowledgment. This work has been supported through a grant from the Petroleum Research Fund, administered by the American Chemical Society. We thank the National Center for Supercomputing Applications (NCSA) at Illinois for providing time on their Power Challenge computer and Prof. W. R. Schowalter (UIUC) for use of his IBM workstation.

References and Notes

(1) Doi, M.; Edwards, S. F. *The Theory of Polymer Dynamics*; Clarendon: Oxford, U.K., 1986.
(2) Allen, M. P.; Tildesley, D. J. *Computer Simulations of Liquids*; Clarendon: Oxford, U.K., 1987.
(3) Knusden, K. D.; Garcia de la Torre, J. *Polymer* **1996**, *37*, 1317.
(4) Binder, K. In *Monte Carlo and Molecular Dynamics Simulations in Polymer Science*; Binder, K., Ed.; Oxford University: New York, 1995.
(5) Freire, J. J.; Pla, J.; Rey, A.; Prats. R. *Macromolecules* **1986**, *19*, 452.
(6) Freire, J. J.; Rey, A.; Bishop, M.; Clarke, J. H. R. *Macromolecules* **1991**, *24*, 6494.
(7) Rodriguez, A. L.; Freire, J. J. *Macromolecules* **1991**, *24*, 3578.
(8) Rey, A.; Freire, J. J.; Bishop, M.; Clarke, J. H. R. *Macromolecules* **1992**, *25*, 1311.
(9) Torres, A. M.; Rubio, A. M.; Freire, J. J.; Bishop, M.; Clarke, J. H. R. *J. Chem. Phys.* **1994**, *100*, 7754.
(10) Milchev, A.; Paul, W.; Binder, K. *J. Chem. Phys.* **1993**, *99*, 4786.
(11) Wittkop, M.; Kreitmeier, S.; Goritz, D. *J. Chem. Phys.* **1996**, *104*, 3373.
(12) Wittkop, M.; Kreitmeier, S.; Goritz, D. *Phys. Rev. E* **1996**, *53*, 838.
(13) Yong, C. W.; Clarke, J. H. R.; Freire, J. J.; Bishop, M. *J. Chem. Phys.* **1996**, *105*, 9699.
(14) Kong, Y.; Manke, C. W.; Madden, W. G.; Schlijper, A. G. *J. Chem. Phys.* **1997**, *107*, 592.
(15) Cathey, C. A.; Fuller, G. G. *J. Non-Newt. Fluid Mech.* **1990**, *34*, 63.
(16) Nguyen, T. Q.; Yu, G.; Kausch, H. H. *Macromolecules* **1995**, *28*, 4851.
(17) Narh, K. A.; Odell, J. A.; Keller, A. *J. Polym. Sci., Polym. Phys. Ed.* **1992**, *30*, 335.
(18) Solomon, M. J.; Muller, S. J. *J. Rheol.* **1996**, *40*, 837.
(19) Hagerman, P. J.; Zimm, B. H. *Biopolymers* **1981**, *20*, 1481.
(20) Andrews, N. C.; McHugh, A. J.; Schieber, J. D. *J. Rheol.* **1998**, *42*, 281.
(21) Öttinger, H. C. *Stochastic Processes in Polymeric Fluids: Tools and Examples for Developing Simulation Algorithms*; Springer-Verlag: Berlin, 1996.
(22) Rotne, J.; Prager, S. *J. Chem. Phys.* **1969**, *50*, 4831.
(23) Wagner, N. J.; Öttinger, H. C. *J. Rheol.* **1997**, *41*, 757.
(24) Bird, R. B.; Curtiss, C. F.; Armstrong, R. C.; Hassager, O. *Dynamics of Polymeric Liquids; Volume 2: Kinetic Theory*, 2nd ed.; Wiley: New York, 1987.
(25) Andrews, N. C.; McHugh, A. J.; Schieber, J. D. *Macromol. Theory Simul.* **1998**, *7*, 19.
(26) Andrews, N. C. Doctoral Thesis, University of Illinois, Urbana, 1997.
(27) Andrews, N. C.; McHugh, A. J.; Schieber, J. D. *J. Polym. Sci., Pt. B: Polym. Phys.* **1998**, *36*.

MA971359J